

On the nature of tunable hole g-factors in quantum dots

N. Ares,¹ V. N. Golovach,^{1,2} G. Katsaros,^{1,2} M. Stoffel,³
F. Fournel,⁴ L. I. Glazman,⁵ O. G. Schmidt,² and S. De Franceschi¹

¹SPSMS, CEA-INAC/UJF-Grenoble 1, 17 Rue des Martyrs, F-38054 Grenoble Cedex 9, France

²Institute for Integrative Nanosciences, IFW Dresden, Helmholtzstr. 20, D-01069 Dresden, Germany

³Université de Lorraine, Institut Jean Lamour, UMR CNRS 7198,
Nancy-Université, BP 239, F-54506 Vandoeuvre-les-Nancy, France

⁴CEA, LETI, MINATEC, 17 Rue des Martyrs, F-38054 Grenoble Cedex 9, France

⁵Department of Physics, Yale University, New Haven, Connecticut 06520, USA

(Dated: November 6, 2018)

Electrically tunable g-factors in quantum dots are highly desirable for applications in quantum computing and spintronics. We report giant modulation of the hole g-factor in a SiGe nanocrystal when an electric field is applied to the nanocrystal along its growth direction. We derive a contribution to the g-factor that stems from an orbital effect of the magnetic field, which lifts the Kramers degeneracy in the nanocrystal by altering the mixing between the heavy and the light holes. We show that the relative displacement between the heavy- and light-hole wave functions, occurring upon application of the electric field, has an effect on the mixing strength and leads to a strong non-monotonic modulation of the g-factor. Despite intensive studies of the g-factor since the late 50's, this mechanism of g-factor control has been largely overlooked in the literature.

In the past decade, a great effort has been devoted to the realization of spin qubits in semiconductors^{1,2}. Spin manipulation was achieved through different approaches: magnetic-field-driven electron spin resonance³, electric-dipole spin resonance⁴⁻⁶, and fast control of the exchange coupling⁷. Another possibility for electric-field spin manipulation is the g-tensor modulation resonance, which has been used on ensembles of spins in two-dimensional (2D) electron systems^{8,9}. This technique relies on anisotropic and electrically tunable g-factors. Recently, several experiments have addressed the g-factor modulation by means of external electric fields^{10,11}, and different mechanisms were evoked to explain the observed g-factor tunability, such as compositional gradients¹⁰ and quenching of the angular momentum^{11,12}. Here we report the experimental observation of an exceptionally large and non-monotonic electric-field modulation of the hole g-factor in SiGe QDs. To interpret this finding we have to invoke a new mechanism that applies to hole-type low-dimensional systems. This mechanism relies on the existence of an important, yet overlooked correction term in the g-factor whose magnitude depends on the mixing of heavy and light holes. We show that in SiGe self-assembled QDs an electric field applied along the growth axis can be used to efficiently alter this mixing and produce large variations in the hole g-factor.

Our SiGe QDs were grown by molecular-beam epitaxy on a silicon-on-insulator substrate. The Stranski-Krastanow growth mode was tuned to yield dome-shaped QDs with height $w = 20$ nm and base diameter $d = 80$ nm. A sketch of the device is shown in Fig. 1 (a). The QD is contacted by two 20-nm-thick Al electrodes, acting as source and drain leads. A Cr/Au gate electrode is fabricated on top of the QD with a 6-nm-thick hafnia interlayer deposited by atomic-layer deposition. This top gate, together with the degenerately-doped Si back gate, allows a perpendicular electric field to be applied while

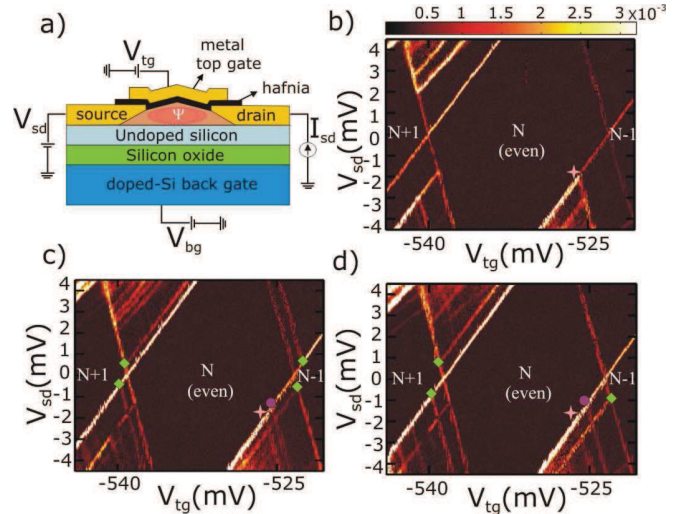


FIG. 1: (a) Schematic cross section of a SiGe QD device. (b)-(d) Color plot of $dI_{sd}/dV_{sd}(V_{tg}, V_{sd})$ for $B_z = 70$ mT, 3 T and 5 T, respectively ($V_{bg} = 0$). The lines indicated by rhombus correspond to the onset of tunneling via Zeeman-split levels for $N - 1$ and $N + 1$ holes on the QD. The lines indicated by a star and by a circle correspond to singlet-triplet excitations for N holes.

maintaining a constant number of holes in the SiGe QD.

Measurements of the g-factor were performed using single-hole tunneling spectroscopy. A typical differential conductance (dI_{sd}/dV_{sd}) measurement as a function of top-gate voltage (V_{tg}) and source-drain bias voltage (V_{sd}) is shown in Fig. 1 (b). All measurements reported here were done in a ³He refrigerator with a base temperature of 250 mK. In order to suppress the superconductivity of the leads, a small magnetic field, $B_z = 70$ mT, was applied along the z axis, i.e. perpendicular to the (x, y) growth plane. Diamond-shaped regions, where the cur-

rent vanishes due to Coulomb blockade, can be clearly observed in Fig. 1 (b). The charging energy is about 10 meV. Outside the diamonds, additional lines denoting transport through excited orbital states can be observed. Figs. 1 (c) and (d) show the same Coulomb-blockade regime for $B_z = 3\text{ T}$ and $B_z = 5\text{ T}$, respectively. The magnetic field causes a splitting of the diamond edges as indicated by green rhombis. This splitting follows from the lifting of Kramers degeneracy in the ground states associated with the side diamonds. We thus conclude that the central diamond corresponds to an even number, N , of confined holes¹. The Zeeman energy splitting is given by $E_Z = g_{\perp}\mu_B B_z$, where μ_B is the Bohr magneton and g_{\perp} is the absolute value of the g-factor along z . From the splitting of N -hole diamond edges we extract $g_{\perp} = (3.0 \pm 0.4)$ and $g_{\perp} = (2.8 \pm 0.4)$ for the $N-1$ and the $N+1$ ground states, respectively. The line indicated by a star in Fig. 1 (b) is due to the spin-triplet excited state for N holes on the QD. We measure a 2 meV singlet-triplet energy in this particular QD, which is an order of magnitude larger than for electrons in Si/SiGe heterostructures¹³. We note that large singlet-triplet excitation energies are particularly desirable for the observation of spin blockade in double-dot experiments¹⁴. Upon increasing B_z , the line denoted by a star splits as shown by the emergence of second parallel line, denoted by a circle, that shifts away proportionally to B_z (see Figs. 1 (c) and (d)). This behavior corresponds to the Zeeman splitting of the excited spin-triplet state¹ with $g_{\perp} = (2.8 \pm 0.4)$. Hereafter, we will concentrate on g-factor measurements in spin-1/2 ground states.

Our dual-gate devices allow us to measure the dependence of the g-factor on a perpendicular electric field, F , at constant number of holes. The principle of such a measurement is illustrated in Fig. 2 (a). The Zeeman splitting is given by the distance between the blue and the red circles along V_{bg} , multiplied by a calibration factor α . The latter is obtained by dividing V_{sd} by the distance between the green and the red circles. In order to investigate the F -dependence of the g-factor, a constant $V_{sd} = 2.6\text{ mV}$ was applied and V_{bg} was swept while stepping V_{tg} . The magnetic field was fixed at 4 T. The data is shown in Fig. 2 (b) and the extracted g-factors are displayed in Fig. 2 (c). We observe an exceptionally large g-factor modulation ($\delta g/g \sim 1$) denoting a strong effect of the applied F . The g-factor increases slowly to a maximum value of 2.6 and then drops rapidly down to a point where the Zeeman splitting can no longer be resolved. Comparably large g-factor variations have been observed in other similar measurements, see Appendix A.

In order to uncover the origin of this unusual behavior, we modelled the QD electronic states in terms of heavy-hole (HH) and light-hole (LH) subbands. Given the relatively large anisotropy of dome-shaped QDs, we initially considered the two-dimensional (2D) limit resulting from confinement along the growth axis. Due to quantum confinement along $z \equiv [001]$ and strain, the 4-fold degeneracy of the valence band at Γ -point is lifted.

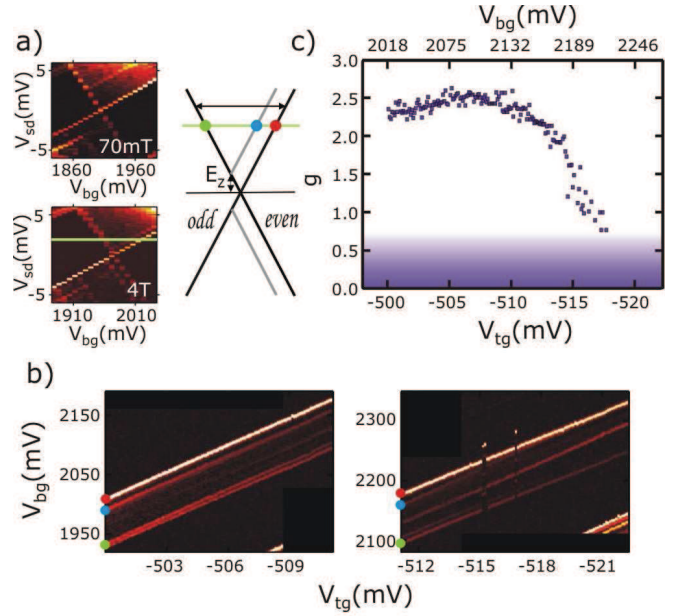


FIG. 2: (a) Left: Color plots of $dI_{sd}/dV_{sd}(V_{bg}, V_{sd})$ for $B = 70\text{ mT}$ and 4 T . At 4 T the Zeeman splitting is clearly visible. Right: Corresponding schematic diagram illustrating the measurement principle to extract the Zeeman energy splitting (and hence the g-factor) from gate-voltage sweeps at constant V_{sd} (see the horizontal green line). (b) Color plots of $dI_{sd}/dV_{sd}(V_{bg}, V_{tg})$ for a fixed $V_{sd} = 2.6\text{ mV}$. These data sets demonstrate the modulation of g_{\perp} by a perpendicular electric field proportional to $V_{bg} - V_{tg}$. (c) $g_{\perp}(V_{bg}, V_{tg})$ as extracted from (b). Below $g_{\perp} \approx 0.75$ the Zeeman splitting cannot be resolved any more due to the finite broadening of the tunneling resonances.

The top-most subband has HH character and its in-plane dispersion relation is described by the effective 2D Hamiltonian

$$H_{\text{eff}} = \frac{1}{2m_{\parallel}} (k_x^2 + k_y^2) + \frac{1}{2}g_{\parallel}\mu_B (\sigma_x B_x + \sigma_y B_y) - \frac{1}{2}g_{\perp}\mu_B \sigma_z B_z + U(x, y), \quad (1)$$

where k_x and k_y are the in-plane momentum operators, $m_{\parallel} = m/(\gamma_1 + \gamma_2)$ is the in-plane effective mass¹⁵, $g_{\parallel} = 3q$ and $g_{\perp} = 6\kappa + \frac{27}{2}q$ are, respectively, the in-plane and transverse g-factors^{15,16}, σ are the Pauli matrices in the pseudospin space¹⁷, and $U(x, y)$ is the in-plane confining potential in the QD. We use standard notations for the Luttinger parameters γ_1 , γ_2 , γ_3 , κ , and q ¹⁸. Since $q \ll \kappa$, it is appropriate to assume $g_{\perp} \approx 6\kappa$. The minus sign in front of $\frac{1}{2}g_{\perp}$ in Eq. (1) is introduced for the convenience of having g_{\perp} positive for Ge.

First we consider the possibility that the observed g-factor modulation arises from a compositional gradient.

It is well known that Si and Ge intermix leading to the formation of a $\text{Si}_{1-x}\text{Ge}_x$ alloy in which x increases monotonically with z , being zero at the base ($z = -w$) and approaching unity at the apex ($z = 0$) of the QD¹⁹. Since

$\kappa_{\text{Si}} = -0.42$ and $\kappa_{\text{Ge}} = 3.41$, one would expect that g_{\perp} increases with F following a vertical shift of the HH wave function towards the apex. This *compositional-gradient* mechanism was exploited in $\text{Al}_x\text{Ga}_{1-x}\text{As}$ quantum wells to implement electrical control of electron spins^{8,9}. While for electrons this may well be the only efficient way to control the g-factor, the situation might be different for holes.

To find an upper bound for the g-factor variation resulting from the compositional gradient, we take the steepest dependence reported for the Ge content across the QD¹⁹,

$$x(z) = x_{\text{max}} \sqrt{1 + \frac{z}{w}}, \quad -w < z < 0, \quad (2)$$

where $w = 20$ nm is the height of the dome-shaped QD. To account for the existing uniaxial strain, we assume that the in-plane lattice constant a_{\parallel} increases linearly from 5.47 Å at the base to 5.59 Å at the apex¹⁹. With these two ingredients, the valence band profiles $E_v(z)$ for all types of holes are calculated using interpolation schemes devised for SiGe ^{20,21} (see inset of Fig. 3). The HH ground state is thus confined to a triangular potential well arising from the compositional gradient. An electric field applied along z adds a term $-eFz$ to $E_v(z)$. For a given F , the HH wave function $\psi(z)$ is obtained by solving the Schrödinger equation numerically. The HH g-factor is found as a weighted average

$$g_{\perp} \approx 6 \langle \kappa \rangle = 6 \int \kappa [x(z)] |\psi(z)|^2 dz, \quad (3)$$

where $\kappa(x)$ is obtained using the non-linear interpolation described in Ref. 22. The resulting dependence $g_{\perp}(F)$ is shown in Fig. 3. We distinguish two regimes: that of a strongly asymmetric (triangular) potential well and that of a symmetric potential well. The modulation of the g-factor is largest in the latter regime (see dotted line in Fig. 3); we obtain $dg_{\perp}/dF \approx 0.41$ m/MV. While the magnitude of the modulation is close to what is observed in the experiment, the sign of dg_{\perp}/dF is nevertheless opposite (see Fig. 2 (c)). We conclude that the compositional-gradient cannot explain our data. Therefore, from now on, we shall discard this mechanism and assume the Ge content to be constant within the QD.

We revisit the derivation of Eq. (1), starting from the Luttinger Hamiltonian. In the 2D limit, the 4×4 Luttinger Hamiltonian separates into 2×2 HH and LH blocks, see Appendix B. To leading order of $w/d \ll 1$, the HH and LH sectors are connected by the off-diagonal mixing blocks²³

$$H_{hl} = (H_{lh})^{\dagger} = i \frac{\sqrt{3}\gamma_3}{m} (k_x \sigma_y + k_y \sigma_x) k_z, \quad (4)$$

where k_x and k_y are 2D versions of momentum operators (insensitive to in-plane magnetic fields), $k_z \equiv -i\hbar\partial/\partial z$, and σ_x and σ_y are the Pauli matrices in a pseudospin

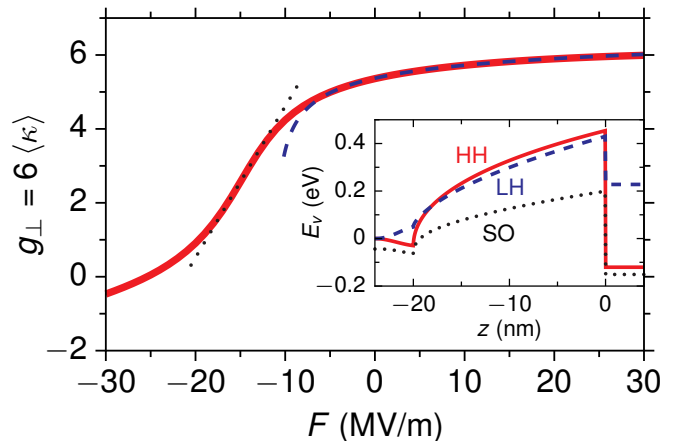


FIG. 3: Expected electric-field dependence of g_{\perp} for a SiGe QD with a strong compositional gradient. The numerical result (solid line) has two regimes, designated by fits to two simplistic models. The dashed line shows a fit to the expression $\langle \kappa \rangle = \kappa_{\infty} - \Delta\kappa(1 + F/F_{\text{intr}})^{-1/3}$, derived for a triangular potential well with an intrinsic electric field F_{intr} for $z < 0$ and infinite barrier for $z > 0$. The dotted line shows a fit to a linear dependence, obtained for a symmetric potential well. In the latter regime, g_{\perp} is most sensitive to F , with $dg_{\perp}/dF = 0.41$ m/MV. At large negative F , the wave function is pushed into the Si-rich region, where g_{\perp} becomes negative. (Inset) Energy profiles for the heavy-hole (HH), light-hole (LH), and split-off (SO) bands for a Ge content x given by Eq. (2) with $x_{\text{max}} = 0.8$. We complemented the QD model with a thin layer of Si substrate at $z \in [-24, -20]$ nm and a strained Si capping layer at $z \in [0, 4]$ nm. Strain is taken into account resulting in a splitting between HH and LH bands.

space, introduced simultaneously for heavy and light holes²³.

The mixing blocks in Eq. (4) are proportional to k_z . In spite of the fact that k_z averages to zero for each type of hole separately, it cannot be discarded in Eq. (4), because matrix elements of the type $\langle \psi_h | k_z | \psi_l \rangle$ are, in general, non-zero and scale as $1/w$ for $w \rightarrow 0$. Here, $\psi_h(z)$ and $\psi_l(z)$ obey two separate Schrödinger equations, for heavy and light holes, respectively (see below). This observation allows us to anticipate that in second-order perturbation theory the mixing blocks lead to an energy correction containing $H_{hl}H_{lh} \propto k_z^2$ in the numerator and $H_{ll} - H_{hh} \propto k_z^2$ in the denominator. This correction does not vanish in the 2D limit ($k_z \rightarrow \infty$). At the same time, the correction to the wave function vanishes as $k_{\parallel}/k_z \sim w/d$.

Using second-order perturbation theory, we recover Eq. (1) for the top-most hole subband. Yet, at the leading (zeroth) order of $w/d \ll 1$, we obtain the following modified expressions for the effective mass and perpendicular g-factor,

$$m_{\parallel} = \frac{m}{\gamma_1 + \gamma_2 - \gamma_h}, \quad g_{\perp} = 6\kappa + \frac{27}{2}q - 2\gamma_h. \quad (5)$$

The in-plane g-factor remains unchanged ($g_{\parallel} = 3q$) at

this order. In Eq. (5), γ_h is a dimensionless parameter sensitive to the form of the confinement along z ,

$$\gamma_h = \frac{6\gamma_3^2}{m} \sum_n \frac{|\langle \psi_n^l | k_z | \psi_1^h \rangle|^2}{E_n^l - E_1^h}. \quad (6)$$

Here, the sum runs over the LH subbands and the wave functions $\psi_n^{h/l}(z)$ and energies $E_n^{h/l}$ obey

$$\left[\frac{k_z^2}{2m_{\perp}^{h/l}} + V_{h/l}(z) \right] \psi_n^{h/l}(z) = E_n^{h/l} \psi_n^{h/l}(z), \quad (7)$$

where $m_{\perp}^{h/l} = m/(\gamma_1 \mp 2\gamma_2)$ and $V_{h/l}(z)$ is the confining potential seen by the heavy/light hole.

When $V_h(z)$ and $V_l(z)$ are infinite square wells, the quantity γ_h in Eq. (6) can be derived analytically,

$$\gamma_h = \frac{12\gamma_3^2}{\gamma_1 + 2\gamma_2} \left[\frac{1}{1 - \beta} - \frac{4\sqrt{\beta}}{\pi(1 - \beta)^2} \cot\left(\frac{\pi}{2}\sqrt{\beta}\right) \right], \quad (8)$$

where $\beta = m_{\perp}^l/m_{\perp}^h + \delta E_{001}/E_1^l$, with $\delta E_{001} \equiv V_h - V_l$ being the splitting of the valence band due to uniaxial strain and $E_1^l = \pi^2 \hbar^2 / 2m_{\perp}^l w^2$. Notably, one has $\psi_n^h(z) = \psi_n^l(z)$ in this case, because the masses m_{\perp}^h and m_{\perp}^l drop out of the expressions for the wave functions. With the application of an electric field, the wave functions ψ_n^h and ψ_n^l begin to shift relative to each other, because of their different effective masses. Although γ_h can only be numerically computed, its qualitative dependence on F can be inferred by inspecting Eq. (6). Note that the $n = 1$ term in the sum has the smallest energy denominator and, therefore, it is expected to have a dominant contribution. For a square-well potential, however, this term vanishes by symmetry. As a result, the symmetric point $F = 0$ corresponds to a minimum in $\gamma_h(F)$, since $E_n^l > E_1^h$. Away from $F = 0$, γ_h increases quadratically, $\gamma_h \propto F^2$, up to the point where the electric field is strong enough to shift the HH wave function ($eFw \simeq E_2^h - E_1^h$). Then, γ_h increases roughly linearly up to the point where the LH wave functions begin to shift ($eFw \simeq E_2^l - E_1^l$). Upon further increasing F , γ_h increases weakly and saturates to a constant. We remark that g_{\perp} is modified by γ_h even at $k_{\parallel} = 0$, despite the fact that no HH-LH mixing occurs at $k_{\parallel} = 0$. In fact, g_{\perp} is sensitive to orbital motion in a perpendicular magnetic field²⁴, and even a small B_z translates to $k_{\parallel} \neq 0$, leading to HH-LH mixing.

Our result in Eq. (5) represents the zeroth-order term in the expansion $g = g^{(0)} + g^{(2)} + \dots$, where $g^{(2)} \propto (w/d)^2$ is the subleading-order term. Unlike the main term, the correction $g^{(2)}$ is sensitive to the in-plane confining potential $U(x, y)$ and it originates from the HH-LH interference terms in the wave function. We shall address $g^{(2)}$ in a separate work. In Fig. 4, we fit the experimental data using only the leading, zero-order term. The insets in Fig. 4 illustrate how the HH and LH wave functions, $\psi_1^h(z)$ (red) and $\psi_1^l(z)$ (blue), shift upon application of the electric field. Note that the transition from the square

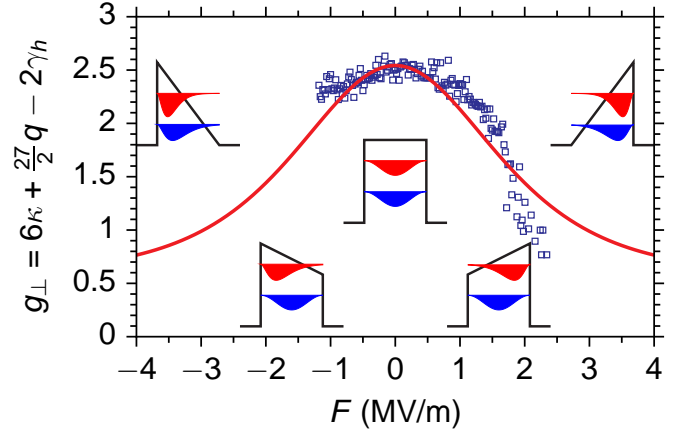


FIG. 4: The $g_{\perp}(F)$ dependence according to Eq. (5) (red line) and corresponding experimental data (open dots). (Insets) Schematics of the HH and LH confinement at different F . The central inset shows the symmetric-well configuration at $F = 0$. The upper insets show the regime of strong F where both types of holes are confined to one side of the (triangular) potential well. The lower insets show the intermediate regime in which F is strong enough to push the heavy hole to one side of the well, while the light hole remains spread over the entire well width.

well (central inset) to the triangular well (upper insets) occurs in two steps. First, the HH wave function shifts by $\delta z \sim w$, while the LH wave function remains nearly unaffected (lowest insets). Then, the LH wave function shifts as well (highest insets). At even larger F (not shown) g_{\perp} saturates to $g_{\perp} \approx 0.6$. The evolution of g_{\perp} taking into account γ_h , shown as a solid red line in Fig. 4, qualitatively reproduces our experimental results (open dots in Fig. 4).

Finally, we remark that the correct 2D limit of the Luttinger Hamiltonian has been largely overlooked in the literature on 2D hole systems. Nevertheless, our main result in Eq. (5) bears some relation to earlier works. D'yakonov and Khaetskii²⁵ studied the Luttinger Hamiltonian in an infinite square well and used the spherical approximation ($\gamma_2 = \gamma_3$). They derived an expression for m_{\parallel} that agrees with our result in the appropriate limit. We also verified that Eqs. (5) and (6) can be obtained from a general $\mathbf{k} \cdot \mathbf{p}$ -approach^{26,27} after a lengthy calculation. In spite of the previous work, however, the relation of m_{\parallel} and g_{\perp} to an additional parameter γ_h and the fact that γ_h is sensitive to F have been missing from the general knowledge of 2D hole systems.

In conclusion, we showed that an external electric field can strongly modulate the perpendicular hole g-factor in SiGe QDs. By a detailed analysis, we ruled out the compositional-gradient mechanism as the origin of this electric-field effect. By analyzing the Luttinger Hamiltonian in the 2D limit, we found a new correction term γ_h which had not been considered before in the literature. This new term, which corrects the “standard” expression for the HH g-factor, reflects the effect of a perpendicular

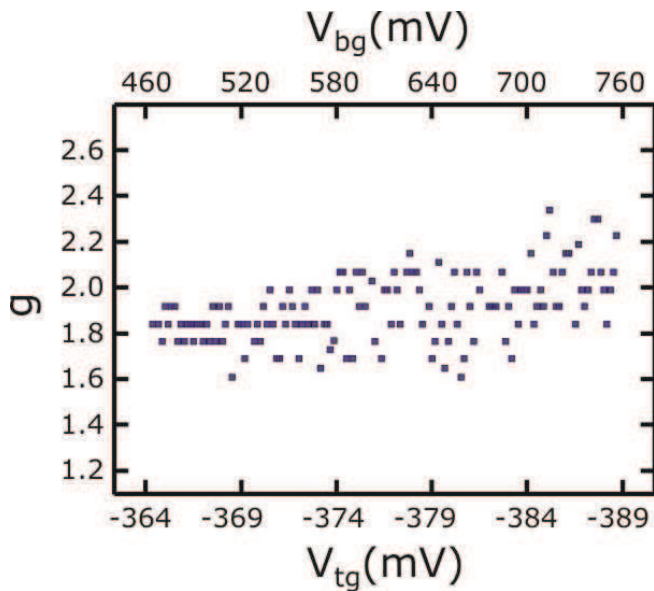


FIG. 5: Measured g-factor versus V_{tg} and V_{bg} for the triangular potential well configuration. The dispersion of the data points is too big to resolve a clear variation in the g-factor value.

magnetic-field on the orbital motion, and it is ultimately related to the atomistic spin-orbit coupling of the valence band.

We acknowledge financial support from the Nanosciences Foundation (Grenoble, France), DOE under the Contract No. DEFG02-08ER46482 (Yale), the Agence Nationale de la Recherche, and the European Starting Grant.

Appendix A: Supplementary data on the g-factor modulation

According to the given theoretical description of the g-factor variation, we should be able to observe a strong effect just when the applied electric field drives the system close to the flat-band configuration. This is the case exhibited in Fig. 4 of the main text. In Fig. 5 the g-factor variation is shown for the same device but in an electric field regime in which the potential well configuration is triangular. Although the range of V_{tg} and V_{bg} is similar in both Fig. 4 and Fig. 5, there is no obvious change in the g-factor value for the latter case, as expected.

It is known that thermal cycling can change the characteristics of a device and thus different set of data can be obtained for the same device²⁸. A drastic change in V_{tg} (of about 3 V) appeared to produce a similar effect in our system. In this way, we could perform the g-factor measurements on two devices with completely different characteristics. This time, a slightly different type of measurement, which will be explained below, was performed in order to extract the g-factors.

As discussed in the main text, by having a dual gate

configuration it is possible to keep the same number of holes while changing the value of the external electric field. The same Coulomb peak can be very easily followed since for each mV we move in V_{tg} , the peaks move ~ 13.2 mV in V_{bg} . This ratio reflects the difference in coupling between the QD and the two gates. Fig. 6 (a) shows how two coulomb peaks shift in V_{bg} while changing V_{tg} from approximately -583 mV (blue trace) to $V_{tg} \simeq -620$ mV (red trace). The reason why the Coulomb peaks appear to be split is that dI_{sd}/dV_{sd} was measured under $V_{sd} = 1$ mV.

By following particular Coulomb peaks we could, for different values of V_{tg} , sweep V_{sd} as a function of V_{bg} , and obtain a stability diagram for the same hole state under different applied electric fields. From the Zeeman-split lines observed in the stability diagrams, we have obtained the g-factors for 11 different values of V_{tg} and V_{bg} , see Fig. 6 (b). The inset which is surrounded by a blue rectangle shows the dI_{sd}/dV_{sd} as a function of (B, V_{sd}) for $V_{tg} \simeq -583.2$ mV. This plot demonstrates that the parallel to the ground state line seen in the stability diagrams insets (orange rectangles), is indeed the Zeeman splitting. From Fig. 6 (b) it becomes clear that the external electric field, has a very strong effect on the g-factor value. It reaches a minimum value of (2.3 ± 0.2) and a maximum value of (3.7 ± 0.4) . This is, to our knowledge, the biggest g-factor value measured in SiGe nanostructures. Even larger g-factors can be obtained for QDs with higher Ge content, as has been shown by theoretical calculations²⁹.

Interestingly, two different behaviours are present in this set of data. From $V_{tg} \approx -560$ to $V_{tg} \approx -630$, the modulation in the g-factor resembles the one shown in the main text. It can be explained by the dependence of γ_h on F . However, from $V_{tg} \approx -630$ to $V_{tg} \approx -660$ an abrupt increase of the g-factor for increasing electric field can be observed. This behaviour is not compatible with the explanation given in the main text. A careful inspection of the stability diagram of Fig. 6 (b) for $V_{tg} \approx -650$ shows that additional levels are present close the studied level. No closely-lying levels are present in the range $V_{tg} \in [-560, -630]$. We believe that the data in the range $V_{tg} \in [-630, -660]$ refers to a different size-quantization level than the data in the range $V_{tg} \in [-560, -630]$. Indeed, the ground-state level might have changed in going from one range to the other, which is presumably signified by the pronounced cusp in the g-factor data at $V_{tg} \approx -630$ mV in Fig. 6 (b). Such transitions are expected to occur when the Fermi level is placed sufficiently deep in the valence band. Then, ladders of levels belonging to different heavy-hole subbands move with respect to each other when the electric field is varied. Since these levels have very different z -components of the wave function, they interact weakly and can come close to each other without a sizable level repulsion. Levels belonging to one ladder cannot come close to each other when the electric field is varied. We therefore speculate that the data in the range $V_{tg} \in [-630, -660]$ refers to a level

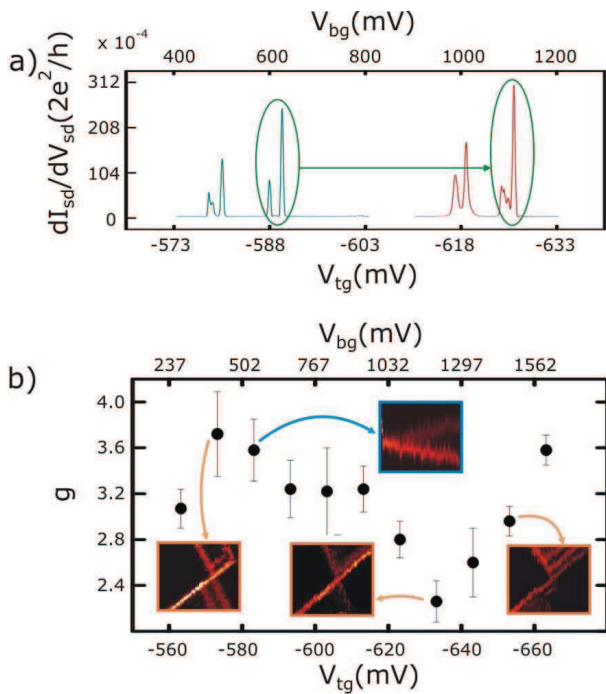


FIG. 6: (a) Plot of dI_{sd}/dV_{sd} versus V_{bg} for $V_{sd} = 1$ mV showing how two coulomb peaks move while changing the value of the external electric field. (b) Plot of the g -factor vs V_{bg} and V_{tg} showing a non monotonic behavior of the g -factor value for different perpendicularly applied electric fields. The insets show stability diagrams at $B = 1.5$ T. V_{bg} is swept by 50 mV while V_{sd} by 2.4 mV. The blue inset demonstrates that indeed the parallel to the ground state line is due to the Zeeman splitting, because it merges with the ground state for vanishing magnetic fields.

from the second heavy-hole subband.

The following question arises: How can the two heavy-hole subbands have different characteristic values of the electric field at which the g -factor reaches maximum. It is important to note that our model in the main text is strongly simplified. The real confining potentials $V_h(z)$ and $V_l(z)$ in the NC are, most likely, never perfectly symmetric and differ from each other. Therefore, it is natural to expect that the alignment along z of wave functions of the two heavy-hole subbands with respect to each other and, at the same time, with respect to the light-hole subbands is not perfect. The data in Fig. 6 (b) is consistent with the assumption that the wave function of the second heavy-hole subband is shifted towards the base of the NC and it begins to align with the light-hole wave functions at a later value of the electric field.

It is important to remark that higher-order corrections to the expansion of the g -factor of the top-most subband cannot explain the abrupt increase taking place for $V_{tg} \in [-630, -660]$, because their contribution is small by $\sim (w/d)^2$, which amounts to only a 10%-correction to the main term for our devices.

Appendix B: The 2D limit of the Luttinger Hamiltonian

Here we derive the expression for γ_h given in Eq. (6) of the main text. Our derivation is based on an expansion of the Luttinger Hamiltonian around the two-dimensional (2D) limit, which we have recently outlined in Ref. 23. We summarize briefly the relevant results of Ref. 23 and address the following question: What is the effective Hamiltonian of the top-most hole subband in the 2D limit?

We start with the representation of the Luttinger Hamiltonian in block form,

$$H = \begin{pmatrix} H_{hh} & H_{hl} \\ H_{lh} & H_{ll} \end{pmatrix}, \quad (\text{B1})$$

where H_{hh} and H_{ll} are the main blocks, describing heavy holes and light holes, respectively. The off-diagonal blocks H_{hl} and $H_{lh} \equiv (H_{hl})^\dagger$ give the mixing between the heavy-hole and light-hole sectors and are responsible for avoided crossings which occur between heavy-hole and light-hole branches at higher energies. The energy axis is chosen to point downwards for holes. In the 2D limit, the heavy-hole and light-hole sectors become well separated in energy and the top-most hole subband (lowest in energy) is described by purely heavy-hole states, i.e. states containing no admixture from the light-hole sector. It is, therefore, customary³⁰ to neglect the off-diagonal blocks in Eq. (B1) when considering the 2D limit and describe the top-most hole subband by an effective Hamiltonian derived only from the block H_{hh} ,

$$H_{\text{eff}} = \langle H_{hh} \rangle, \quad (\text{B2})$$

where $\langle \dots \rangle$ stands for averaging over the motion along z . Contrary to the common expectation, Eq. (B2) does not describe correctly the 2D limit of the Luttinger Hamiltonian. The correct expression in the place of Eq. (B2) involves terms of the order of H_{hl}^2/H_{ll} , which remain finite in the 2D limit. While these terms do not change the qualitative picture of the result, they are important when mechanisms of electric control of the g -factor and effective mass are considered.

Before proceeding further we need to clarify what exactly we mean by the 2D limit. By the 2D limit of the Luttinger Hamiltonian, we mean a limit in which the z -sizes of both heavy-hole and light-hole wave functions are sent to small values, e.g. by means of confining the holes to a thin layer of material. Of course, the Luttinger Hamiltonian is by itself an effective Hamiltonian (intended for top of valence band) and it is valid only for energies much smaller than the spin-orbital energy Δ_{SO} . However, Δ_{SO} is, typically, a large energy and one can envision the following limit,

$$E \ll \Delta_z \ll \Delta_{SO}, \quad (\text{B3})$$

where E is the energy measured away from the edge of the top-most subband and $\Delta_z \sim (\gamma_2/m) \langle k_z^2 \rangle$ is the splitting

energy between heavy and light holes due to confinement (or due to strain if strain dominates). We, therefore, have in mind Eq. (B3) when talking about the 2D limit of the Luttinger Hamiltonian. It is important to note that, in the Luttinger Hamiltonian¹⁸, Δ_{SO} is already sent to infinity and, thus, the second inequality in Eq. (B3) is, formally, fulfilled within the model. In practice, however, our derivation remains qualitatively correct up to $\Delta_z \lesssim \Delta_{\text{SO}}$. For Ge, one has $\Delta_{\text{SO}} \approx 0.3$ eV.

After expanding the Luttinger Hamiltonian in terms of the small parameter $w/d \ll 1$ (see Ref. 23), the main blocks in Eq. (B1) are given at the leading order by

$$\begin{aligned} H_{hh} &= \frac{\gamma_1 + \gamma_2}{2m} (k_x^2 + k_y^2) + \frac{\gamma_1 - 2\gamma_2}{2m} k_z^2 \\ &\quad + \frac{1}{2} \mu_B \boldsymbol{\sigma} \cdot g_h \cdot \mathbf{B} + U(x, y) + V_h(z), \\ H_{ll} &= \frac{\gamma_1 - \gamma_2}{2m} (k_x^2 + k_y^2) + \frac{\gamma_1 + 2\gamma_2}{2m} k_z^2 \\ &\quad + \frac{1}{2} \mu_B \boldsymbol{\sigma} \cdot g_l \cdot \mathbf{B} + U(x, y) + V_l(z), \end{aligned} \quad (\text{B4})$$

where k_x and k_y are the 2D momentum operators, which contain only the z -component of the magnetic field. The inplane components of the magnetic field contribute to H at higher orders of the expansion, but not at the leading order considered here. The g -factors, g_h and g_l , entering Eq. (B4), are diagonal in the frame (x, y, z) and given by

$$g_h = \begin{pmatrix} 3q & 0 & 0 \\ 0 & 3q & 0 \\ 0 & 0 & -6\kappa - \frac{27}{2}q \end{pmatrix}, \quad (\text{B5})$$

and

$$g_l = \begin{pmatrix} 4\kappa + 10q & 0 & 0 \\ 0 & 4\kappa + 10q & 0 \\ 0 & 0 & 2\kappa + \frac{1}{2}q \end{pmatrix}. \quad (\text{B6})$$

The confining potential is assumed to separate into an inplane component $U(x, y)$ and a transverse $V_{h/l}(z)$. The confining potential can be different for heavy and light holes, because of the strain.

The off-diagonal blocks are related to each other by hermiticity,

$$H_{hl} = (H_{lh})^\dagger. \quad (\text{B7})$$

For H_{lh} , we keep the leading-order term

$$H_{lh} = -i \frac{\sqrt{3}\gamma_3}{m} (k_x \sigma_y + k_y \sigma_x) k_z. \quad (\text{B8})$$

In writing Eq. (B4) and (B8), we made a choice of basis for the hole pseudo-spin. We chose the basis such that the pseudo-spin transforms under the time-reversal operation as a spin 1/2, see Ref. 23,

$$\begin{aligned} |\uparrow\rangle_h &= |3/2, -3/2\rangle, & |\downarrow\rangle_h &= |3/2, +3/2\rangle, \\ |\uparrow\rangle_l &= |3/2, +1/2\rangle, & |\downarrow\rangle_l &= |3/2, -1/2\rangle. \end{aligned} \quad (\text{B9})$$

This choice of basis is convenient since it allows us to have ‘‘standard’’ time-reversal transformations for all operators. In Eq. (B9), we use basis of states of the angular momentum $J = 3/2$ ³¹:

$$\begin{aligned} \left| \frac{3}{2}, +\frac{3}{2} \right\rangle &= -\frac{1}{\sqrt{2}} (X + iY) \uparrow, \\ \left| \frac{3}{2}, -\frac{3}{2} \right\rangle &= \frac{1}{\sqrt{2}} (X - iY) \downarrow, \\ \left| \frac{3}{2}, +\frac{1}{2} \right\rangle &= \frac{1}{\sqrt{6}} [-(X + iY) \downarrow + 2Z \uparrow], \\ \left| \frac{3}{2}, -\frac{1}{2} \right\rangle &= \frac{1}{\sqrt{6}} [(X - iY) \uparrow + 2Z \downarrow], \end{aligned} \quad (\text{B10})$$

where the functions X , Y , and Z are real and represent the Bloch amplitudes of the valence band in the absence of spin-orbit interaction.

Next, we rotate away the off-diagonal blocks in Eq. (B1) using perturbation theory³². We are allowed to do so if we focus on a heavy hole state which is far away from any light hole states. This requirement is fulfilled in an energy window between the edges of the first heavy-hole and light-hole subbands, i.e. close to the top of the valence band. Of course, occasionally, such a premise may hold for a state deep in the valence band. And, in particular, it may hold for a light-hole state. In the latter case, we would be deriving an effective Hamiltonian in the favour of the light hole. However, the majority of states deep in the valence band do not permit application of perturbation theory.

In order to quantify the applicability of our method, we introduce characteristic values for the momenta operators in a localized state:

$$\bar{k}_\alpha^h = \sqrt{\langle h | k_\alpha^2 | h \rangle}, \quad (\alpha = x, y, z), \quad (\text{B11})$$

where $|h\rangle$ stands for the localized (heavy-hole) state. Then, the expansion around the 2D limit (i.e. separation of variables) is valid if

$$\bar{k}_{x,y}^h \ll \bar{k}_z^h, \quad (\text{B12})$$

whereas the perturbation theory can be applied if

$$\frac{\gamma_3}{m} \sqrt{\bar{k}_{x,y}^h \bar{k}_{x,y}^l} \ll E_l - E_h, \quad \forall l, \quad (\text{B13})$$

where the index l refers to the light-hole states. Here, E_h and E_l are energies of the heavy-hole and light-hole states, respectively. Since we restrict our consideration to small inplane momenta, we can approximate E_h and E_l by

$$\begin{aligned} E_h &\approx \frac{\gamma_1 - 2\gamma_2}{m} \langle k_z^2 \rangle_h, \\ E_l &\approx \frac{\gamma_1 + 2\gamma_2}{m} \langle k_z^2 \rangle_l, \end{aligned} \quad (\text{B14})$$

where $\langle k_z^2 \rangle_{h/l}$ is the average of k_z^2 with the z -component of the wave function. With this approximation, the energy denominator in expressions of perturbation theory

reads

$$E_l - E_h = \frac{\gamma_1}{2m} (\langle k_z^2 \rangle_l - \langle k_z^2 \rangle_h) + \frac{\gamma_2}{m} (\langle k_z^2 \rangle_l + \langle k_z^2 \rangle_h). \quad (\text{B15})$$

It is important to remark here that this energy denominator does not depend on the quantum numbers of the inplane motion. To simplify the notations above, we denoted all the quantum numbers by a single index, h (or l). Below, we shall single out the quantum number referring to the z -component of the wave function. Thus, we shall replace $E_l - E_h$ in Eq. (B15) by $E_n^l - E_{n_0}^h$, where n and n_0 denote quantum numbers of the motion along z and the superscripts h and l indicate to which type of hole the expression belongs. The z -components of wave functions associated with subband energies E_n^l and $E_{n_0}^h$ are denoted by $\psi_n^l(z)$ and $\psi_{n_0}^h(z)$, respectively.

We average over the motion along z and obtain

$$H_{\text{eff}} = \langle H_{hh} \rangle + \langle \Delta H_{hh} \rangle, \\ \langle \Delta H_{hh} \rangle = - \sum_n \langle \psi_{n_0}^h | H_{hl} | \psi_n^l \rangle \frac{1}{E_n^l - E_{n_0}^h} \langle \psi_n^l | H_{lh} | \psi_{n_0}^h \rangle, \quad (\text{B16})$$

where $\langle \dots \rangle \equiv \langle \psi_{n_0}^h | \dots | \psi_{n_0}^h \rangle$ and n_0 denotes the number of the heavy-hole subband for which we derive the effective 2D Hamiltonian. In practice, n_0 can be one of the several first subbands and in the main text we set $n_0 = 1$. Further, the derivation continues as follows,

$$\langle \Delta H_{hh} \rangle = - \sum_n \frac{\langle \psi_{n_0}^h | k_z | \psi_n^l \rangle \langle \psi_n^l | k_z | \psi_{n_0}^h \rangle}{E_n^l - E_{n_0}^h}$$

$$\times \frac{3\gamma_3^2}{m^2} (k_x \sigma_y + k_y \sigma_x)^2. \quad (\text{B17})$$

Next, note that

$$(k_x \sigma_y + k_y \sigma_x)^2 = k_x^2 + k_y^2 - i [k_x, k_y] \sigma_z. \quad (\text{B18})$$

Since $[k_x, k_y] = -i(\hbar e/c)B_z$, we obtain

$$\langle \Delta H_{hh} \rangle = -\frac{\gamma_{h,n_0}}{2m} \left(k_x^2 + k_y^2 - \frac{e\hbar}{c} \sigma_z B_z \right), \quad (\text{B19})$$

where

$$\gamma_{h,n_0} = \frac{6\gamma_3^2}{m} \sum_n \frac{\langle \psi_{n_0}^h | k_z | \psi_n^l \rangle \langle \psi_n^l | k_z | \psi_{n_0}^h \rangle}{E_n^l - E_{n_0}^h}. \quad (\text{B20})$$

Therefore, we obtained a g-factor renormalization and a mass renormalization. The heavy-hole g-factor g_z changes to

$$g_{z,n_0} = -6\kappa - \frac{27}{2}q + 2\gamma_{h,n_0}. \quad (\text{B21})$$

The inplane mass reads

$$m_{\parallel,n_0}^h = \frac{m}{\gamma_1 + \gamma_2 - \gamma_{h,n_0}}. \quad (\text{B22})$$

-
- ¹ R. Hanson, L.P. Kouwenhoven, J.R. Petta, S. Tarucha, and L.M.K. Vandersypen, *Rev. Mod. Phys.* **79**, 1217 (2007).
² D. Loss, and D. DiVincenzo, *Phys. Rev. A* **57**, 120 (1998).
³ F.H.L. Koppens, C. Buizert, K.J. Tielrooij, I.T. Vink, K.C. Nowack, T. Meunier, L.P. Kouwenhoven, and L.M.K. Vandersypen, *Nature* **442**, 766 (2006).
⁴ K.C. Nowack, F.H.L. Koppens, Yu.V. Nazarov, and L.M.K. Vandersypen, *Science* **318**, 1430, (2007).
⁵ S. Nadj-Perge, S.M. Frolov, E.P.A.M. Bakkers, and L.P. Kouwenhoven, *Nature* **468**, 1084 (2010).
⁶ V.N. Golovach, M. Borhani, and D. Loss, *Phys. Rev. B* **74**, 165319 (2006).
⁷ J.R. Petta, A.C. Johnson, J.M. Taylor, E.A. Laird, A. Yacoby, M.D. Lukin, C.M. Marcus, M.P. Hanson, A.C. Gos-sard, *Science* **309**, 2180 (2005).
⁸ Y. Kato, R.C. Myers, D.C. Driscoll, A.C. Gossard, J. Levy, and D.D. Awschalom, *Science* **299**, 1201 (2003).
⁹ G. Salis, Y. Kato, K. Ensslin, D.C. Driscoll, A.C. Gossard, and D.D. Awschalom, *Nature* **414**, 619 (2001).
¹⁰ R.S. Deacon, Y. Kanai, S. Takashashi, A. Oiwa, K. Yoshida, K. Shibata, K. Hirakawa, Y. Tokura, and S. Tarucha, *Phys. Rev. B* **84**, 041302 (2011).
¹¹ V. Jovanov, T. Eissfeller, S. Kapfinger, E.C. Clark, F. Klotz, M. Bichler, J.G. Keizer, P.M. Koenraad, G. Abstreiter, and J.J. Finley, *Phys. Rev. B* **83**, 161303 (2011).
¹² C.E. Pryor and M.E. Flatté, *Phys. Rev. Lett.* **96**, 026804 (2006).
¹³ N. Shaji, C.B. Simmons, M. Thalukulam, L.J. Klein, H. Qin, H. Luo, D.E. Savage, M.G. Lagally, A.J. Rimberg, R. Joynt, M. Friesen, R. Blick, S.N. Coppersmith, and M.A. Eriksson, *Nature Phys.* **4**, 540 (2008).
¹⁴ K. Ono, D.G. Austing, Y. Tokura, and S. Tarucha, *Science* **297**, 1313 (2002).
¹⁵ R. Winkler, *Spin-Orbit Coupling Effects in Two-Dimensional Electron and Hole Systems* (Springer, New York, 2003).
¹⁶ H.W. van Kesteren, E.C. Cosman, and W.A.J.A. van der Poel, *Phys. Rev. B* **41**, 5283 (1990).
¹⁷ We choose the pseudospin basis as in Ref. 23; namely, $|\uparrow\rangle_h = |3/2, -3/2\rangle$ and $|\downarrow\rangle_h = |3/2, +3/2\rangle$.
¹⁸ J.M. Luttinger, *Phys. Rev.* **102**, 1030 (1956).
¹⁹ T.U. Schüllli, M. Stoffel, A. Hesse, J. Stangl, R.T. Lechner, E. Wintersberger, M. Sztucki, T.H. Metzger, O.G. Schmidt, and G. Bauer, *Phys. Rev. B* **71**, 035326 (2005).
²⁰ C.G. Van de Walle and R.M. Martin, *Phys. Rev. B* **34**, 5621 (1986).
²¹ M.M. Rieger and P. Vogl, *Phys. Rev. B* **48**, 14276 (1993).
²² R. Winkler, M. Merkler, T. Darnhofer, and U. Rössler, *Phys. Rev. B* **53**, 10858 (1996).
²³ G. Katsaros, V.N. Golovach, P. Spathis, N. Ares, M. Stoffel, F. Fournel, O.G. Schmidt, L.I. Glazman, and S. De Franceschi, *Phys. Rev. Lett.* **107**, 246601 (2011).

- ²⁴ K.A. Matveev, L.I. Glazman, and A.I. Larkin, Phys. Rev. Lett. **85**, 2789 (2000).
- ²⁵ M.I. D'yakonov and A.V. Khaetskii, Sov. Phys. JETP **55**, 917 (1982).
- ²⁶ L. Roth, B. Lax, and S. Zwerdling, Phys. Rev. **114**, 90 (1959).
- ²⁷ A.A. Kiselev, E.L. Ivchenko, and U. Rössler, Phys. Rev. B **58**, 16353 (1998).
- ²⁸ C. Buizert, A. Oiwa, K. Shibata, K. Hirakawa, and S. Tarucha, Phys. Rev. Lett. **99**, 136806 (2007).
- ²⁹ A.V. Nenashev, A.V. Dvurechenskii, and A.F. Zinovieva, Phys. Rev. B **67**, 205301 (2003).
- ³⁰ P.Y. Yu, M. Cardona, *Fundamentals of Semiconductors: Physics and Materials Properties*, 4th Edition, (Springer-Verlag Berlin Heidelberg, 2010).
- ³¹ V.N. Abakumov, V.I. Perel, and I.N. Yassievich, *Nonradiative Recombination in Semiconductors*, (North-Holland, 1991).
- ³² L.D. Landau and E.M. Lifshitz, *Quantum Mechanics: Non-relativistic theory*, (Pergamon Press, 1977).